Nanoscale

PAPER

View Article Online
View Journal | View Issue

Cite this: *Nanoscale*, 2019, **11**, 5754

# Investigation of high contrast and reversible luminescence thermochromism of the quantum confined $Cs_4PbBr_6$ perovskite solid†

Jin Woo Choi, ‡[a] Namchul Cho,‡[b] Hee Chul Woo, [a] Byeong M. Oh,[c] Jawaher Almutlaq,[d] Osman M. Bakr,[d] Sung-Hoon Kim,*[e] Chang-Lyoul Lee *[a] and Jong H. Kim *[b]

Received 19th December 2018,
Accepted 15th February 2019

DOI: 10.1039/c8nr10223f

rsc.li/nanoscale

Thermochromism of organic/inorganic halide perovskites has attracted particular interest due to their potential applications as photoluminescence (PL)-based temperature sensors. However, despite the outstanding PL characteristics, their use as a thermochromic material in practical temperature ranges has been limited because of their poor thermal stability. In this study, we used the quantum confinement effect and exceptional PL quantum efficiency of the $Cs_4PbBr_6$ perovskite to demonstrate their high on/off ratio (20) and reversible PL thermochromism in the solid state in practical temperature ranges including room temperature (RT). Systematic photophysical and optical characterization studies, including exciton–phonon scattering, exciton binding energy, exciton decay dynamics, and crystal structure change, were performed to investigate the origin of this unique thermochromic PL property. The results showed that the efficient and highly reversible thermochromic PL emission of the $Cs_4PbBr_6$ perovskite is due to its desirable optical properties such as highly luminescent emission, efficient PL quenching at high temperatures, and thermally reversible structural changes.

## Introduction

Stimuli-responsive photoluminescent (PL) materials have been widely researched for their applications in optical sensors, emission switches, and drug delivery systems.[1–7] Thermochromic PL, known as reversible PL emission changes either in intensity or emission wavelength in response to temperature variations, is of particular interest because of its potential applications in luminescent thermometers.[8–11] To demonstrate efficient luminescence switching, solid-state thermochromic materials should possess a high luminescence contrast between the ON and OFF states in practical temperature ranges. This can be realized by developing high PL quantum yield (PLQY) materials, which also exhibit extremely suppressed radiative PL decay in the OFF state when exposed to temperatures higher than the threshold temperature.

Recently, organic/inorganic hybrid perovskites (HPVs) have emerged as highly promising functional materials because of their exceptional optoelectronic properties.[12–15] Some HPVs have also been reported to exhibit thermochromic colour changes due to their temperature-dependent phase transition characteristics.[16–20] However, the low PLQY and poor thermal stability of HPV films challenge their applications as thermochromic PL materials. Fortunately, the poor thermal stability can be overcome by replacing the organic component with an inorganic component (*e.g.*, cesium), and the low PLQY can be enhanced by increasing the exciton binding energy through reducing the structural dimensionality of the perovskites.[21–25] Zero-dimensional $CsPbX_3$ (X = Cl, Br, I) quantum dots (QDs) exhibit a high PLQY (>90%) in a solution with high thermal stability. However, severe quenching of the PLQY occurs in the solid state due to aggregation between the QDs, causing a blinking effect and Auger recombination, which hinders their practical thermochromic applications.[25–28] Recently, the $Cs_4PbBr_6$ perovskite featuring a high PLQY in the solid state (~45%) has been developed, where the $[PbBr_6]^{4-}$ octahedra are surrounded by Cs, which prevents interactions among the

---

[a] *Advanced Photonics Research Institute (APRI), Gwangju Institute of Science and Technology (GIST), Gwangju, 61005, Republic of Korea. E-mail: vsepr@gist.ac.kr*
[b] *Department of Energy Systems, Soonchunhyang University, Asan 31538, Republic of Korea. E-mail: jonghkim@ajou.ac.kr*
[c] *Department of Molecular Science and Technology, Ajou University, Suwon 16499, Republic of Korea*
[d] *King Abdullah University of Science and Technology (KAUST), KAUST Solar Center, Physical Sciences and Engineering Division (PSE), Thuwal 23955-6900, Saudi Arabia*
[e] *Department of Textile System Engineering, Kyungpook National University, Daegu, 702-701 Republic of Korea. E-mail: shokim@knu.ac.kr*

† Electronic supplementary information (ESI) available. See DOI: 10.1039/c8nr10223f

‡ These authors contributed equally to this work.

$Pb^{2+}$ ions.[29–32] In this zero-dimensional structure, Br vacancy defects ($[PbBr_5]^{3-}$) contribute to a midgap (green) radiative state due to the relevant energy level.[33] In contrast to the conventional structured $CsPbX_3$ QD films that exhibit dynamic interparticle interactions, the $Cs4PbX_6$ perovskite structure retains, even in its films, its high PLQY property due to the atomic separation of the $Pb^{2+}$ sites. Motivated by the excellent PLQY of $Cs_4PbBr_6$ in the solid state, we investigated its thermochromism and the underlying mechanisms through the characterization analyses of the optical properties and crystal structures. Moreover, unlike $CsPbBr_3$, the $Cs_4PbBr_6$ perovskite exhibits a high fluorescence contrast and reversibility in the applied temperature range.

## Results and discussion

The pure $Cs_4PbBr_6$ and $CsPbBr_3$ perovskites used in this study were synthesized and purified following a published process.[29,30] The UV-Vis absorption spectrum in Fig. 1(a) showing the absorption edge at ~540 nm is well matched with a reported absorption spectrum of $Cs_4PbBr_6$.[29] The absence of a powder X-ray diffraction (PXRD) peak between 14 and 18° confirmed the absence of $CsPbBr_3$ in the synthesized $Cs_4PbBr_6$ sample (Fig. 4(a)). Furthermore, the calculated crystal structure from the $d$ values of PXRD peaks was a trigonal structure with a lattice parameter of $a = b = 14.1$ and $c = 17.5$ Å. These results confirm the successful preparation of a highly pure monophasic rhombohedral $Cs_4PbBr_6$ crystal (JPCDS no. 73-2478).[30–32]

The morphology of $Cs_4PbBr_6$ in the solid state was investigated by using scanning electron microscopy (SEM) measurements in which ~10 μm sized particles were aggregated as the bulk state (Fig. 1(b)). As shown in Fig. 1(c), the PL emission of $Cs_4PbBr_6$ in the solid state gradually disappeared (OFF state) as the substrate temperature was increased from 25 to 100 °C, and appeared (ON state) as the substrate was cooled to 25 °C, confirming the reversibility of the emission. The PL emission intensity contrast ($I_{on}/I_{off}$) of $Cs_4PbBr_6$ in this practical temperature range is visible to the naked eye. This is in sharp contrast to the behavior of $CsPbBr_3$ in the solid state (the reference perovskite), which exhibited a weak and irreversible PL emission intensity in the same temperature range.

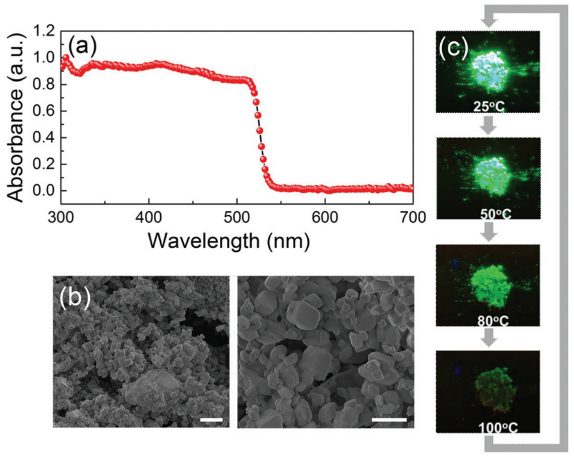

Fig. 1 (a) Absorption spectrum, (b) SEM images of pure $Cs_4PbBr_6$ in the solid state (scale bars: 20 μm), and (c) photographic images of thermochromic behaviour.

To understand the difference between the emission properties of the two perovskites, we further investigated the radiative and non-radiative exciton relaxation dynamics of $CsPbBr_3$ and $Cs_4PbBr_6$ in the solid state through temperature-dependent PL measurements (Fig. 2). The PL intensity change at different temperatures is presented in Fig. 2(a) (note that the gradually blue-shifted emission wavelength with the increased temperature is due to the lattice dialation).[40] Fig. 2(b) presents the integrated PL intensity in the temperature range of 20–420 K in which the intensity values at 300 ($I_{on}$) and 420 K ($I_{off}$) were extracted for the calculation of $I_{on}/I_{off}$ ratios for $CsPbBr_3$ (3.3) and $Cs_4PbBr_6$ (20). The high $I_{on}/I_{off}$ value for $Cs_4PbBr_6$ is attributed to the combined effects of the highly luminescent nature of $Cs_4PbBr_6$ (PLQY: ~45%) in the ON state and the efficient PL quenching in the OFF state.

For a detailed investigation of the exciton dynamics in ON/OFF states, the steady-state PL spectra as a function of temperature were fitted by using eqn (S1) and (S2) (Fig. S1†).[34] In the PL intensity fitting of $CsPbBr_3$, the parameters for the thermal escape of the exciton by longitudinal optical (LO) phonon absorption were eliminated due to the continuous energy band diagram. The extracted exciton–phonon coupling strength for acoustic phonons ($\gamma_{ac}$), exciton–phonon coupling strength for optical phonons ($\gamma_{LO}$), exciton binding energy ($E_b$), and phonon energy ($E_{LO}$) are listed in Table 1. For both $Cs_4PbBr_6$ and $CsPbBr_3$ perovskites, the negligibly small values of $\gamma_{ac}$ indicate that the effects of acoustic phonon scattering on the PL characteristics can be ignored, compared to the other effects, which include the quantum confinement effect, the optical phonon-induced thermal escape effect, and the trap-induced exciton quenching effect.

The $Cs_4PbBr_6$ perovskite exhibited a much higher $E_b$ of 368 meV than the $CsPbBr_3$ perovskite (73 meV) due to the quantum confinement effect (eqn (S2)†). The higher $E_b$ of $Cs_4PbBr_6$ enabled a high PL intensity in the ON state by reducing exciton thermal dissociation.[34,35] This ON state changes to the OFF state when the excitons are dissociated by overcoming the $E_b$, as the applied temperature increases. Because of the high $E_b$, $Cs_4PbBr_6$ shows a higher thermochromic threshold temperature near the RT (~300 K), compared to $CsPbBr_3$ (~30 K), as shown in Fig. 2(b).

The origin of non-radiative exciton relaxation dynamics in the OFF state at high temperatures can be explained by comparing the non-radiative strength of shallow trap-related thermal activation ($Ae^{-E_a/k_BT}$), exciton dissociation ($Be^{-E_b/k_BT}$), and optical phonon related thermal escape of charge carriers ($C(e^{-E_{LO}/k_BT}-1)^{-m}$) in eqn (S2).† Fig. 2(c) and (d) show the non-radiative decay strength of these terms in $CsPbBr_3$ and $Cs_4PbBr_6$ perovskites. In the case of $CsPbBr_3$, the maximum PL intensity at ~30 K is quenched to ~10% of the initial intensity

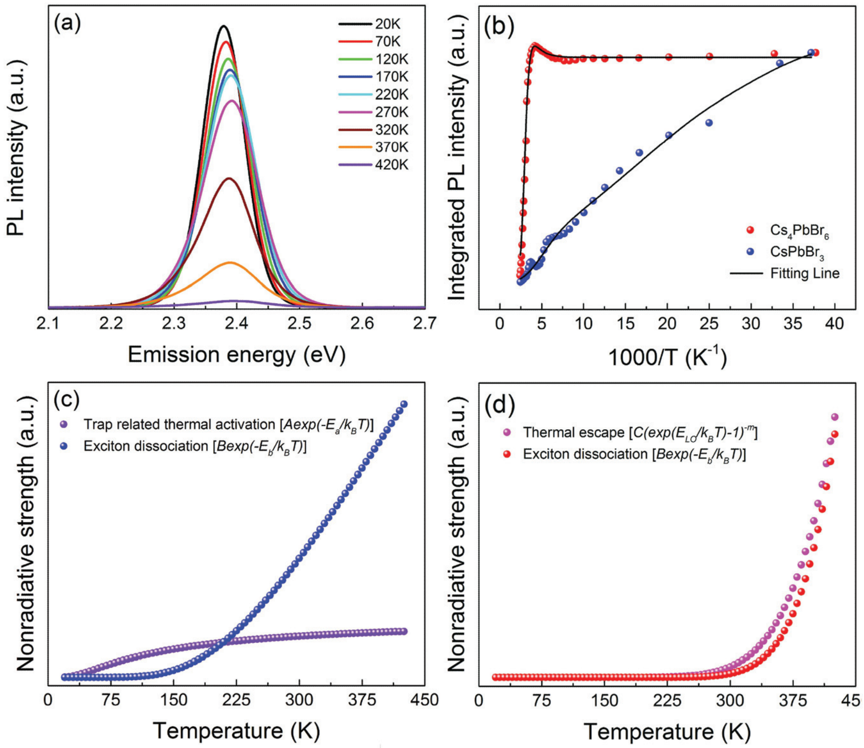

**Fig. 2** (a) Temperature-dependent PL spectra of $Cs_4PbBr_6$ and (b) integrated PL intensity of $CsPbBr_3$ and $Cs_4PbBr_6$. Non-radiative decay strength comparison for: (c) $CsPbBr_3$ and (d) $Cs_4PbBr_6$.

**Table 1** Calculated exciton–phonon coupling strength for acoustic phonons ($\gamma_{ac}$), exciton–phonon coupling strength for optical phonons ($\gamma_{LO}$), exciton binding energy ($E_b$), and phonon energy ($E_{LO}$) of $Cs_4PbBr_6$ and $CsPbBr_3$ perovskites

| Perovskites | $\gamma_{ac}$ (meV) | $\gamma_{LO}$ (meV) | $E_b$ (meV) | $E_{LO}$ (meV) |
|---|---|---|---|---|
| $Cs_4PbBr_6$ | 0.0804 | 123 | 368 | 62 |
| $CsPbBr_3$ | 0.0001 | 259 | 73 | 23 |

at 150 K. Furthermore, the strength of the exciton dissociation is observed to rapidly increase at temperatures higher than 120 K, while the strength of trap-related thermal activation is saturated at 150 K after a gradual increase (Fig. 2(c)). In contrast to the general explanation that the PL quenching of the perovskites is due to efficient exciton dissociation, our observations on the trap-related thermal activation and exciton dissociation strength indicate that the main non-radiative exciton decay pathway in the $CsPbBr_3$ thermochromic film is the trap-related thermal activation in all temperature ranges including high temperatures where exciton dissociation becomes dominant. Compared to $CsPbBr_3$, the $Cs_4PbBr_6$ perovskite shows an abrupt increment in both optical phonon-related thermal escape of charge carriers and exciton dissociation in the high temperature region without any saturation as shown in Fig. 2(d). Both non-radiative decay strengths have a similar threshold temperature and are observed to allow dramatic suppression of radiative exciton recombination at temperatures higher than the thermochromic threshold temperature in the $Cs_4PbBr_6$ film.

Time-correlated single-photon counting (TCSPC) measurements were performed at the maximum PL intensity peak ($\lambda_{max}$: 520 nm) for different temperatures to elucidate the exciton relaxation dynamics in $Cs_4PbBr_6$ as presented in Fig. 3. The PL decay curves were analyzed by using tri-exponential fitting. The lifetimes ($\tau$) and fractional intensities ($f$) for fast, middle-decay ($\tau_1, f_1, \tau_2, f_2,$) induced by radiative recombination and thermal stimuli related slow-decay ($\tau_3$, $f_3$) components

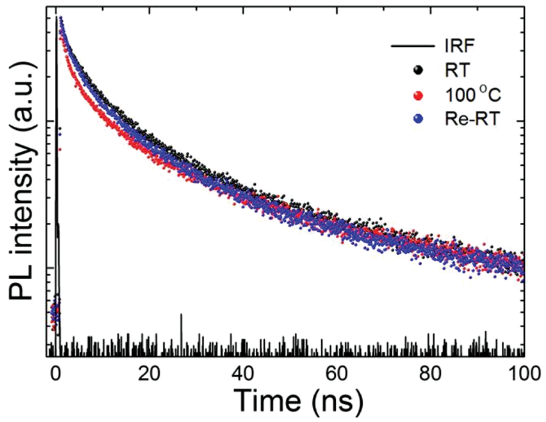

**Fig. 3** PL decay profiles of $Cs_4PbBr_6$ with IRF at different substrate temperatures.

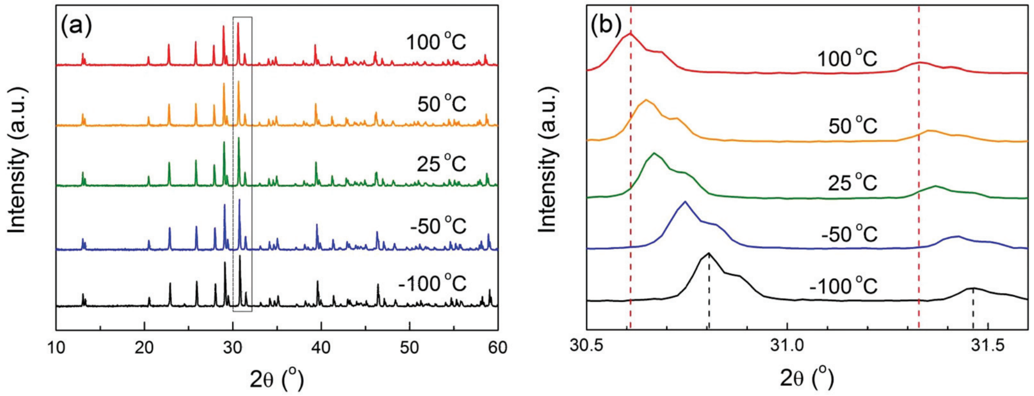

**Fig. 4** (a) PXRD patterns of $Cs_4PbBr_6$ in the solid state at different substrate temperatures and (b) magnified view of the gradual shift of diffraction peaks at the corresponding temperatures.

were extracted from the fitting process (Table S2†). The middle-decay ($\tau_2$, $f_2$) fraction was considered as radiative recombination because the Br vacancy defects ($[PbBr_5]^{3-}$) contributed radiative states in $Cs_4PbBr_6$.[1] As expected, the $\tau_1$ value for $Cs_4PbBr_6$ decreased from 1.80 to 1.31 ns due to the efficient thermal escape of carriers and exciton dissociation at 100 °C and it returned to its original value after the subsequent cooling to 25 °C. The $\tau_2$ and its fraction ($f_2$) presented similar behaviour depending on the temperature changes. In contrast, thermal stimuli related slow-decay ($\tau_3$, $f_3$) components were increased from 43.00 to 44.50 ns, and then reversibly returned to 43.01 ns during the cyclic temperature change from 25, 100 to 25 °C. The observed reversible thermochromic emission characteristics suggest reversible changes in the phase transition of the perovskite rather than structural destruction.[36,37] To investigate the structural changes of $Cs_4PbBr_6$, we monitored the temperature-dependent PXRD patterns of $Cs_4PbBr_6$ in the solid state from −100 to 100 °C, as shown in Fig. 4. Interestingly, all the observed diffraction peaks showed a gradual and reversible shift depending on the applied temperatures. As can be seen in Fig. 4(b), for example, the (223) peak is observed to shift from 30.8 to 30.6° when the temperature is increased from −100 to 100 °C. The result indicates an increase of *d*-spacing values due to the thermal expansion of the lattice. This expansion induced tensile stress on the $Cs_4PbBr_6$ resulting in a blue-shift of PL emission and quenched emission intensity of $Cs_4PbBr_6$.[38–40] Therefore, the thermochromic luminescence of $Cs_4PbBr_6$ is not only associated with exciton dissociation dynamics, but also closely related to reversible structural changes by thermal-induced structural stress on the crystal lattice.

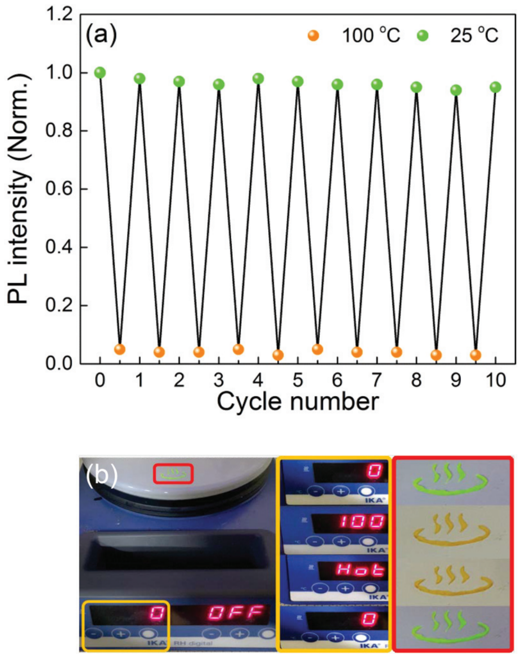

**Fig. 5** (a) PL intensity of the $Cs_4PbBr_6$ film during repeated heating (100 °C) and cooling (25 °C) cycles. (b) Photographic images of the temperature-dependent $Cs_4PbBr_6$ ink pattern.

As shown in Fig. 5(a), reversible PL thermochromism behavior was clearly observed due to the temperature-dependent PL intensity of $Cs_4PbBr_6$. Such an optical characteristic suggests the utilization of $Cs_4PbBr_6$ for temperature monitoring systems. Finally, the application of $Cs_4PbBr_6$ as a temperature sensor was investigated. As shown in Fig. 5(b), we printed $Cs_4PbBr_6$ having a hot spring mark on the hotplate. The intensity of emission from the printed $Cs_4PbBr_6$ pattern at room temperature reduced with increased temperature to 100 °C (hot).

## Conclusions

In this study, we have investigated the high contrast (20) thermochromic PL of perovskites by using zero-dimensional $Cs_4PbBr_6$ in the solid state. Photophysical and structural analyses have been performed to investigate the underlying reasons for this unique behavior. The results showed that the high $I_{on}/I_{off}$ of $Cs_4PbBr_6$ in the solid state is due to the combined effects of the highly luminescent nature of $Cs_4PbBr_6$ in the ON state (high exciton binding energy) and efficiently suppressed PL emission in the OFF state (high thermal escape of charge carriers and exciton dissociation). Moreover, $Cs_4PbBr_6$ was observed to undergo a temperature-induced reversible phase transition, which allows reversible PL emission ON–OFF, depending on the applied temperatures. Based on the unique properties and useful functions in luminescence, these perovskites are expected to have potential applicability in practical sensors including luminescent thermometers.

## Conflicts of interest

There are no conflicts to declare.

## Acknowledgements

This research was supported by the Basic Science Research Program through the National Research Foundation of Korea (NRF), funded by the Ministry of Education (2018R1D1A1B07047645). This research was also supported by the Global Infrastructure Program through the National Research Foundation of Korea (NRF) funded by the Ministry of Science and ICT (2018K1A3A1A17081404). This research was also supported by the National Research Foundation of Korea (NRF), grant funded by the Korean Government, Ministry of Science and ICT (MSIP) (NRF-2016R1A2B4013003, NRF-2018R1A2A3075144 and NFR-2017R1C1B5017953) and a grant funded by GIST 2019 (Research on Advanced Optical Science and Technology).

## Notes and references

1 W.-E. Lee, C.-L. Lee, T. Sakaguchi, M. Fujiki and G. Kwak, *Macromolecules*, 2011, **44**, 432–436.

2 S.-C. Lee, J. Heo, J.-W. Ryu, C.-L. Lee, S. Kim, J.-S. Tae, B.-O. Rhee, S.-W. Kim and O.-P. Kwon, *Chem. Commun.*, 2016, **52**, 13695–13698.

3 P. C. Chen, J. Y. Ma, L. Y. Chen, G. L. Lin, C. C. Shih, T. Y. Lin and H. T. Chang, *Nanoscale*, 2015, **6**, 3503–3507.

4 G. Luo, L. Shen, J. Zheng and C. Xu, *J. Mater. Chem. C*, 2017, **5**, 3488–3494.

5 M. K. Panda, N. Ravi, P. Asha and A. P. Prakasham, *CrystEngComm*, 2018, **20**, 6046–6053.

6 J. Wang, T. Kumeria, M. T. Bezem, J. Wang and M. J. Sailor, *ACS Appl. Mater. Interfaces*, 2018, **10**, 3200–3209.

7 F. Chen, P. Huang, Y. J. Zhu, J. Wu, C. L. Zhang and D. X. Cui, *Biomaterials*, 2011, **32**, 9031–9039.

8 J. Huo, Z. Hu, G. He, X. Hong, Z. Yang, S. Luo, X. Ye, Y. Li, Y. Zhang, M. Zhang, H. Chen, T. Fan, Y. Zhang, B. Xiong, Z. Wang, Z. Zhu and D. Chen, *Appl. Surf. Sci.*, 2017, **423**, 951–956.

9 D. Sun, S. Yuan, H. Wang, H. F. Lu, S. Y. Feng and D. F. Sun, *Chem. Commun.*, 2013, **49**, 6152–6154.

10 R. Toivola, T. Howie, J. Yang, P.-N. Lai, Z. Shi, S.-H. Jang, A. K.-Y. Jen and B. D. Flinn, *Smart Mater. Struct.*, 2017, **26**, 085039.

11 D. Yan, J. Lu, J. Ma, M. WAei, D. G. Evans and X. Duan, *Angew. Chem., Int. Ed.*, 2011, **50**, 720–723.

12 M. M. Lee, J. Teuscher, T. Miyasaka, T. N. Murakami and H. J. Snaith, *Science*, 2012, **338**, 643–647.

13 M. Xiao, F. Huang, W. Huang, Y. Dkhissi, Y. Zhu, J. Etheridge, A. Gray-Weale, U. Bach, Y. B. Cheng and L. A. Spiccia, *Angew. Chem.*, 2014, **126**, 10056–10061.

14 W. S. Yang, B. W. Park, E. H. Jung, N. J. Jeon, Y. C. Kim, D. U. Lee, S. S. Shin, J. Seo, E. K. Kim, J. H. Noh and S. I. Seok, *Science*, 2017, **356**, 1376–1379.

15 A. Kogo, Y. Sanehira, Y. Numata, M. Ikegami and T. Miyasaka, *ACS Appl. Mater. Interfaces*, 2018, **10**, 2224–2229.

16 P. S. Whitfield, N. Herron, W. E. Guise, K. Page, Y. Q. Cheng, I. Milas and M. K. Crawford, *Sci. Rep.*, 2016, **6**, 35685.

17 H. Yu, Z. Wei, Y. Hao, Z. Liang, Z. Fu and H. Cai, *New J. Chem.*, 2017, **41**, 9586–9589.

18 M. Bastiani, M. I. Saidaminov, I. Dursun, L. Sinatra, W. Peng, U. Buttner, O. F. Mohammed and O. M. Bakr, *Chem. Mater.*, 2017, **29**, 3367–3370.

19 A. Halder, D. Choudhury, S. Ghosh, A. S. Subbiah and S. K. Sarkar, *J. Phys. Chem. Lett.*, 2015, **6**, 3180–3184.

20 J. Lin, M. Lai, L. Dou, C. S. Kley, H. Chen, F. Peng, J. Sun, D. Lu, S. A. Hawks, C. Xie, F. Cui, A. P. Alivisatos, D. T. Limmer and P. Yang, *Nat. Mater.*, 2018, **17**, 261–267.

21 M. Kulbak, S. Gupta, N. Kedem, I. Levine, T. Bendikov, G. Hodes and D. Cahen, *J. Phys. Chem. Lett.*, 2016, **7**, 167–172.

22 X. Chang, W. Li, L. Zhu, H. Liu, H. Geng, S. Xiang, J. Liu and H. Chen, *ACS Appl. Mater. Interfaces*, 2016, **8**, 33649–33655.

23 Y. Chen, Y. Sun, J. Peng, J. Tang, K. Zheng and Z. Liang, *Adv. Mater.*, 2018, **30**, 1703487.

24 M. G. La-Placa, G. Longo, A. Babaei, L. Martinez-Sarti, M. Sessolo and H. J. Bolink, *Chem. Commun.*, 2017, **53**, 8707–8710.

25 H. Huang, L. Polavarapu, J. A. Sichert, A. S. Susha, A. S. Urban and A. L. Rogach, *NPG Asia Mater.*, 2016, **8**, e328.

26 J. W. Choi, H. C. Woo, X. Huang, W. G. Jung, B. J. Kim, S. W. Jeon, S. Y. Yim, J. S. Lee and C.-L. Lee, *Nanoscale*, 2018, **10**, 13356–13367.

27 X. Du, G. Wu, J. Cheng, H. Dang, K. Ma, Y.-W. Zhang, P.-F. Tan and S. Chen, *RSC Adv.*, 2017, **7**, 10391–10396.

28 S. Seth, N. Mondal, S. Patra and A. Samanta, *J. Phys. Chem. Lett.*, 2016, **7**, 266–271.

29 M. I. Saidminov, J. Almutlaq, S. Sarmah, I. Dursun, A. A. Zhumekenov, R. Begum, J. Pan, N. Cho, O. F. Mohammed and O. M. Bakr, *ACS Energy Lett.*, 2016, **1**, 840–845.

30 Y. Zhang, M. I. Saidaminov, I. Dursun, H. Yang, B. Murali, E. Alarousu, E. Yengel, B. A. Alshankiti, O. M. Bakr and O. F. Mohammed, *J. Phys. Chem. Lett.*, 2017, **8**, 961–965.

31 J. H. Cha, J. H. Han, W. Yin, C. Park, Y. Park, T. K. Ahn, J. H. Cho and D. Y. Jung, *J. Phys. Chem. Lett.*, 2017, **8**, 565–570.

32 D. Chen, Z. Wan, X. Chen, Y. Yuan and J. Zhong, *J. Mater. Chem. C*, 2016, **4**, 10646–10653.

33 J. Yin, H. Yang, K. Song, A. M. El-Zohry, Y. Han, O. M. Bakr, J. L. Bredas and O. F. Mohammed, *J. Phys., Lett.*, 2018, **9**, 5490–5495.

34 H. C. Woo, J. W. Choi, J. Shin, S. H. Chin, M. H. Ann and C.-L. Lee, *J. Phys. Chem. Lett.*, 2018, **9**, 4066–4074.

35 Z. Yang, M. Wang, H. Qiu, X. Yao, X. Lao, S. Xu, Z. Lin, L. Sun and J. Shao, *Adv. Funct. Mater.*, 2018, **28**, 1705908.

36 S. Kumar, A. Qadir, F. Maury and N. Bahlawane, *ACS Appl. Mater. Interfaces*, 2017, **9**, 21447–21456.

37 H. Liu, L. Yuan, S. Wang, H. Fang, Y. Zhang, C. Hou and S. Feng, *J. Mater. Chem. C*, 2016, **4**, 10529–10537.

38 A. Lazarowska, S. Mahlik, M. Grinberg, G. Li and R. S. Liu, *Sci. Rep.*, 2016, **6**, 34010.

39 M. E. Aumer, S. F. LeBoeuf, S. M. Bedair, M. Smith, J. Y. Lin and H. X. Jiang, *Appl. Phys. Lett.*, 2000, **77**, 821.

40 J. Yin, Y. Zhang, A. Bruno, C. Soci, O. M. Bakr, J.-L. Brédas and O. F. Mohammed, *ACS Energy Lett.*, 2017, **2**, 2805–2811.